Processing and Application of Ceramics 14 [2] (2020) 146–153
https://doi.org/10.2298/PAC2002146A

Structure, electric and dielectric properties of $PbFe_{1/3}Ti_{1/3}W_{1/3}O_3$ single perovskite compound

Patnala Ganga Raju Achary[1], Ram Narayan Prasad Choudhary[2], Santosh Kumar Parida[2,*]

[1]*Department of Chemistry, ITER, Siksha O Anusandhan, Deemed to be University, Khandagiri Square, Bhubaneswar - 751030 India*
[2]*Department of Physics, ITER, Siksha 'O' Anusandhan, Deemed to be University, Khandagiri, Square, Bhubaneswar - 751030 India*

Received 21 November 2019; Received in revised form 7 March 2020; Received in revised form 10 April 2020; Accepted 16 April 2020

Abstract

A conventional solid-state method was used to prepare $Pb(Fe_{1/3}Ti_{1/3}W_{1/3})O_3$ single perovskite material. The sample sintered at 900 °C was studied by XRD and after Rietveld refinement the orthorhombic structure with Pbam space group was confirmed. The FTIR frequency bands corresponding to Pb–O, Ti–O, O-lattice, W–O–W and Fe–O stretching vibrations together with the XRD data also confirmed that Fe^{2+} and W^{6+} ions are incorporated in the structure and most probably substituted Ti^{4+} ions at the B site of the perovskite ABO_3 structure. The average grain size of the perovskite ceramics, estimated from SEM micrograph, was 1 to 2 μm. Variation of dielectric properties and AC conductivity with frequency and temperature revealed that the material had semiconducting nature and negative temperature coefficient of resistance (NTCR). The Nyquist plots were modelled with an equivalent circuit consisted of parallel capacitance, resistance and constant phase element corresponding to the grains (bulk) and grain boundaries. It was observed that grain resistance (R_b) of the sample decreases with the rise of temperature, which supports the NTCR behaviour. The semi-circular arcs of the Nyquist and Cole-Cole plots confirm the semiconducting nature of the sample.

Keywords: *perovskite, multiferroic, electrical properties, AC conductivity, permittivity, Nyquist plots*

I. Introduction

There are different types of material structures, out of which perovskite and tungsten bronze are found to have the best piezoelectric and ferroelectric properties available in nature. Thus, people showed great interest in studying perovskite structures because of anomalous structures which can be obtained by doping. Particularly, the advantages of perovskite structure are its flexibility of choosing different types of cations for substitution on both A and B sites without much change of the structure and also making the complete solid solution with many cations over a wide range of compositions. It is important for a material scientist to give updated information about different new materials (starting with their chemical composition, constituent phases, and microstructure) that come on the market because of the demand for technological applications from manufacturing units.

Most of the industries require well-developed materials to work with, process monitoring and quality assurance. The relevant electrical properties of a material play a vital role to decide its applications. The precise electrical measurements of a sample can provide scientists and engineers useful knowledge which can be incorporated to enhance the properties of the materials, thereby increasing the demand for fundamental science and various technological applications. In this context, the dielectric measurement of material can provide crucial design parameters for many applications in electronic industry. For example, the impedance of a substrate, dielectric relaxor, frequency of the resonator and cable insulator are directly related to the dielectric measurements [1,2]. It is well known in the literature that information on the dielectric properties of a given mate-

* Corresponding author: tel: +91 9861406462,
e-mail: *santoshparida@soa.ac.in*

rial is very useful to enhance the ferrite, absorber, packaging and design capacity [3–5]. Nowadays, the basic information of the dielectric properties of a material can be applied to well-defined areas such as aerospace, automotive, food and medical industries [6–12]. The readjustment of the atoms, molecules, and defects in the materials due to the external electric field to attend equilibrium state is called dielectric relaxation, which depends on the lattice properties, frequency and temperature. The dielectric relaxation can be used to study the molecular interactions in polar liquids and also study H-bond in liquids [13–16]. The value of the dielectric constant of a material can be used to separate polar solvents from non-polar solvents by reducing solute's internal charge.

A lot of researches have directed their research on the particular group of materials called ferroelectrics, having a high dielectric constant and low tangent loss, which shows the non-linearity and exhibits hysteresis of *P-E* curve [17–19]. The exceptional characters of the ferroelectric materials are the spontaneous polarization, reversibility, anomalous physical properties and structural modification at the transition temperature [20]. The presence of the above interesting properties makes the ferroelectric materials extremely useful for different device fabrication: i) the high dielectric constant ferroelectric materials are good for energy storage capacitors, ii) a good ferroelectric hysteresis may be useful for non-volatile memories, iii) high piezoelectric value may be useful in making electronic devices such as sensors, actuators and resonant wave devices such as radio-frequency filters, iv) high pyroelectric coefficients may be useful in making infra-red detectors, v) the strong electro-optic effects may be useful in making optical switches and vi) anomalous temperature coefficients of the resistivity may be used in electric-motor overload protection circuits [21–23].

Physical and chemical properties of a perovskite compound have to be understood before considering how to enhance the inherent properties of the materials and use them in different devices. The single $Pb(Fe_{1/3}Ti_{1/3}W_{1/3})O_3$ (PFTW) perovskite compound is known for its good dielectric properties, but it is still an interesting area of research as evident from the literature [24]. Thus, in this paper, structure and electrical properties of $Pb(Fe_{1/3}Ti_{1/3}W_{1/3})O_3$ perovskite compound have been discussed in detail. The results and discussion of the samples show some interesting properties and indicate on practical applications.

II. Experimental

A conventional solid-state method was used to prepare the $Pb(Fe_{1/3}Ti_{1/3}W_{1/3})O_3$ single perovskite compound material. In the first step, high purity metal oxides (PbO, FeO, TiO_2 and WO_3) were mixed in appropriate weight ratio to meet the stoichiometry of $PbFe_{1/3}Ti_{1/3}W_{1/3}O_3$ perovskite compound. In the second step, an agate mortar and pestle were used to homogenise the metal oxides mixture manually for 2–3 h. Wet-grinding with methanol followed for at least 2 h for additional particle size reduction and more effective homogenisation. In the third step, the sample was calcined at different temperatures (starting from 600 °C) in a temperature programmed furnace and the formation of the compound was constantly checked by XRD (using D8 Advance of M/s Bruker Co with λ = 1.5405 Å). If the compound was not formed or no solid state reaction took place, the reaction mixture was further ground and calcination temperature was increased. Finally, at 850 °C the reaction took place and the formation of the desirable compound was ascertained by the XRD analysis. Then the powder sample was used to make 10 mm diameter and 2 mm thickness circular pellets. The pressed PFTW samples were sintered at three different temperatures 850, 900 and 950 °C and the respective densities of the sintered samples were calculated from the geometry and the mass of the sample [25]. The densities of the $Pb(Fe_{1/3}Ti_{1/3}W_{1/3})O_3$ perovskite sintered at 850, 900 and 950 °C were 7.75, 7.87 and 7.88 g/cm^3, respectively. Since the pellets were sintered well enough at 900 °C, this sample was selected for further analyses.

Before the electrical measurement, both sides of the circular sample were silver painted and heated up to 150 °C for 2 h to eliminate the residual moisture. The electrical continuity of both sides of the silvered sample was checked using a multi-meter. The LCR (Phase Sensitive Meter, PSM) was used to measure the electrical parameters of the sample, which includes relative dielectric constant (ε_r), tangent loss (tan δ), AC conductivity (σ_{AC}), impedance (Z), etc. by scanning between 1 kHz and 1 MHz from room temperature to 500 °C.

III. Results and discussion

3.1. Structure

Figure 1 represents the XRD profile of the PFTW single perovskite compound. The Rietveld refinement of

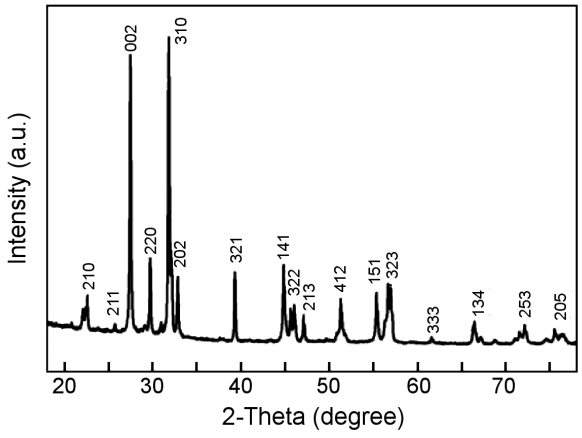

Figure 1. XRD profile of the $PbFe_{1/3}Ti_{1/3}W_{1/3}O_3$ single perovskite compound

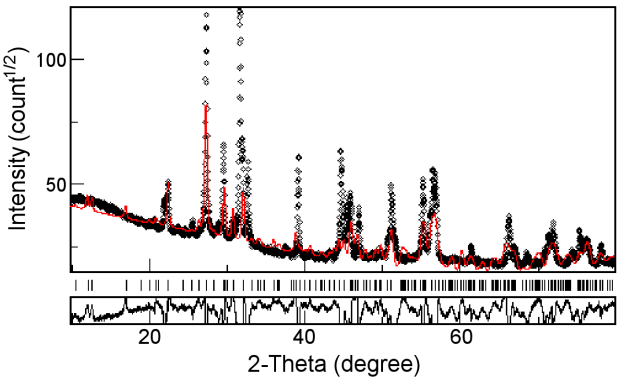

Figure 2. XRD pattern with Rietveld refinement of the $PbFe_{1/3}Ti_{1/3}W_{1/3}O_3$ single perovskite compound

the experimental XRD data was done by using MAUD software [26]. The presence of all existing XRD peaks is closely matched with standard crystal data corresponding to the JCPDS file No. 01-086-0109 and confirm that the sample has orthorhombic crystal structure with *Pbam* space group. There is no second phase formed because of the absence of extra XRD peaks [27,28]. Figure 2 represents the XRD pattern of the sample with Rietveld refinement carried out by using the Pseudo-Voigt function [29]. The calibration of the refinement of peaks was done by changing the presence of different simulation parameters, i.e. FWHM, shape parameters, zero shift, background scale factor, lattice parameters, specimen displacement, preferred orientation, transparency, atomic positions and anisotropic temperature parameters [30]. The refined cell parameters are a = 9.305 Å, b = 9.247 Å, c = 5.67 Å and $\alpha = \beta = \gamma = 90°$. The reliability factors obtained from the Rietveld refinement are $R_{wp}(\%)$ = 15.55, $R_{exp}(\%)$ = 3.31, $R_B(\%)$ = 14, and $GOF = (\chi)^2$ = 4.63 which are well-matched with the literature data.

Figure 3a represents FTIR spectrum of the PFTW single perovskite compound. The frequency band at 499 cm^{-1} corresponds to Pb–O stretching [31–33]; frequency band at 518 cm^{-1} corresponding to Ti–O stretching [34]; the band at 538 cm^{-1} corresponds to O-lattice stretching [35,36]; the bands at 623 cm^{-1} and 695 cm^{-1} correspond to W–O–W stretching [37] and frequency band at 651 cm^{-1} corresponds to Fe–O stretching [38,39]. These results confirm that Fe^{2+} and W^{6+} ions are incorporated in the structure and most probably substituted the Ti^{4+} ions in the B site of the perovskite ABO_3 structure as also confirmed by the XRD data. Figure 3b represents the SEM micrograph of the PFTW single perovskite compound. The average grain size estimated from SEM micrograph is from 1 to 2 μm.

3.2. Dielectric properties

Figures 4a and 4b represent the variation of the dielectric constant with a wide range of frequency (form 1 kHz to 1 MHz) and temperatures (from 25 to 500 °C). The dielectric constant (ε_r) of a sample provides the ability to store energy when a suitable electric potential is applied across the sample. The dielectric constant of a sample depends on the two factors, i.e. polarization vector and capacitance. For small scale electrical devices, materials with a higher value of the dielectric constant (ε_r) are always chosen. It is observed that dielectric constant of the sintered PFTW sample decreases with frequency increase. At low frequency range, dielectric constant increases considerably with the rise of temperature from 25 to 500 °C. Figure 4b shows that ε_r gradually increases with the increase in temperature, passes through a maximum which is moved towards higher temperature. This transition could be attributed to some kind of relaxor ferro- or antiferroelectric behaviour [40]. This peak basically disappears with increasing frequency, which is the typical relaxor-ferroelectric behaviour. This interesting ferroelectric transition is known to take place in the steps: i) from paraelectric to ferroelectric and ii) ferroelectric to relaxor ferroelectric. The peak around ~300 °C due to the existence of the ferroelectric transition is also observed in the tangent loss curves (Fig. 5b). This result reveals that the prepared material may be a

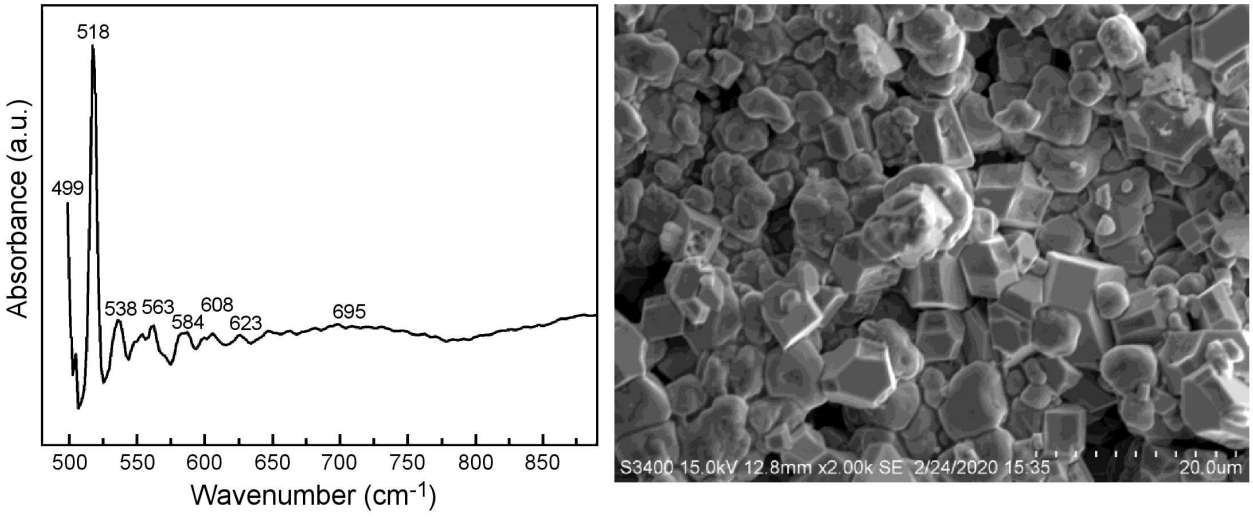

Figure 3. FTIR spectrum (a) and SEM image (b) of the $PbFe_{1/3}Ti_{1/3}W_{1/3}O_3$ single perovskite compound

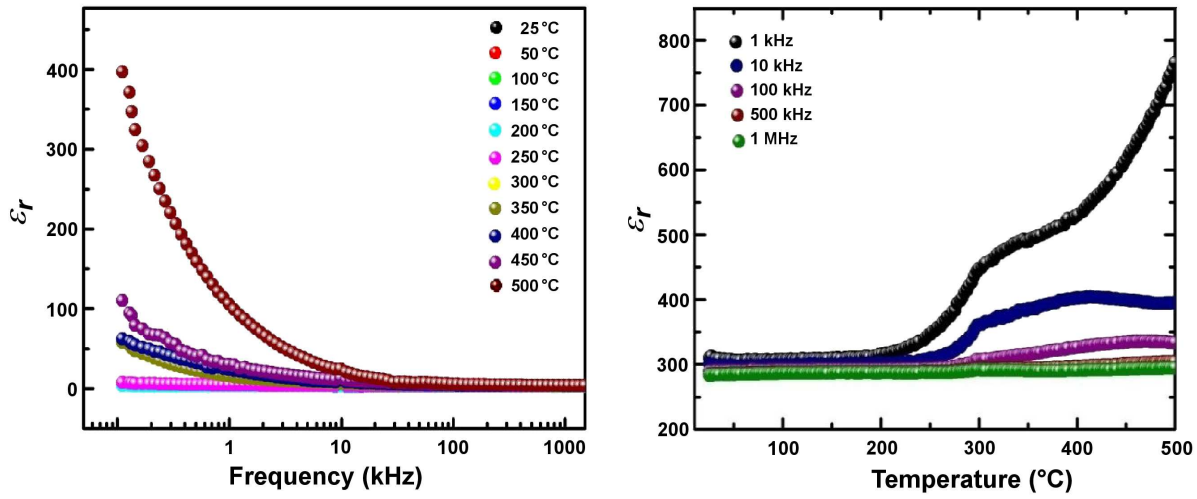

Figure 4. Variation of dielectric constant with frequency (a) and temperature (b)

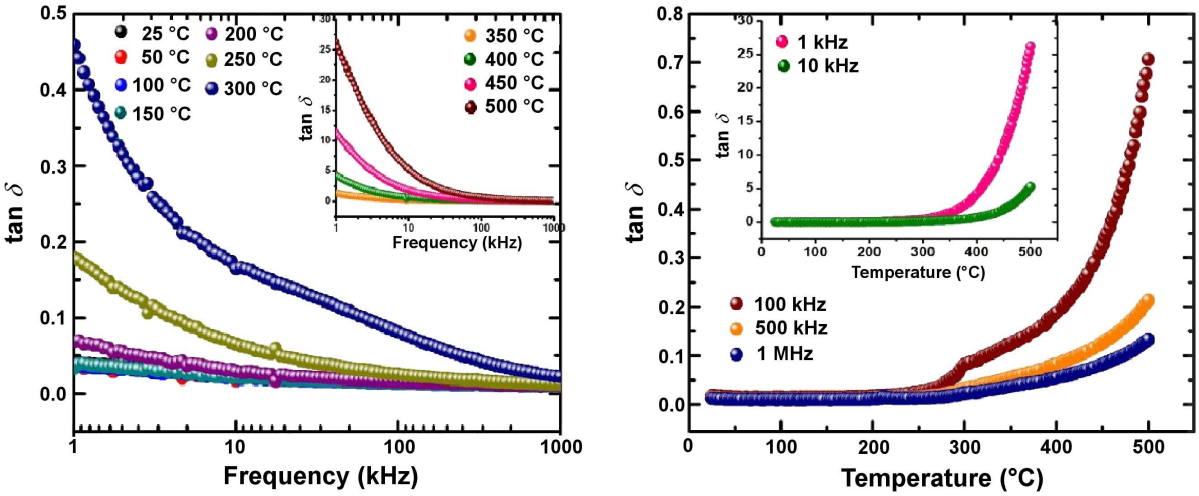

Figure 5. Variation of tangent loss with frequency (a) and temperature (b)

good candidate for energy storage devices at low frequency range of applied AC electric field. Similarly, at the higher range of temperature, the dielectric constant of the sample decreases with frequency supporting the energy storage ability.

Figures 5a and 5b represent the variation of the tangent loss with frequency (from 1 kHz to 1 MHz) and temperature (from 25 to 500 °C). Tangent loss ($\tan\delta$) of a material gives the idea of electrical energy loss due to the conduction, dielectric relaxation, dielectric resonance and loss from non-linear processes [41]. The preliminary development of the dielectric loss in a material may be due to mismatching of the frequency of the applied electric field with electric displacement vectors. There are two types of dielectric losses seen in materials. Those that come from the crystal symmetry, frequency of applied AC electric field and temperature are called extrinsic losses, whereas combined effects of impurities, structural defects, grain boundaries, micro-cracks, dislocations and vacancies are called intrinsic losses. In the present study, at lower range of frequency, the dielectric losses of the sintered PFTW sample increase with the rise of temperature, but at higher range of temperatures $\tan\delta$ decreases with the rise of frequency. The weak peak around ~300 °C could be also clearly seen in tangent loss curves (Fig. 5b). So, the prepared sample is a potential material for device fabrication for energy storage.

3.3. Impedance analyses

Figures 6a and 6b represent the variation of the real and imaginary part of impedance in the wide range of frequency at different temperatures from 25 to 500 °C. Both curves show a decreasing tendency which confirms that the material becomes more conducting, so the sample has NTCR character, i.e. semiconducting nature. At different temperatures, both Z' and Z'' curves merging in a high frequency range specify the release of space charge, which may be the cause for the decrease of the barrier properties [42]. The observed relaxation in low-temperature region may be due to the electron mobility while oxygen vacancies or defects may be possible rea-

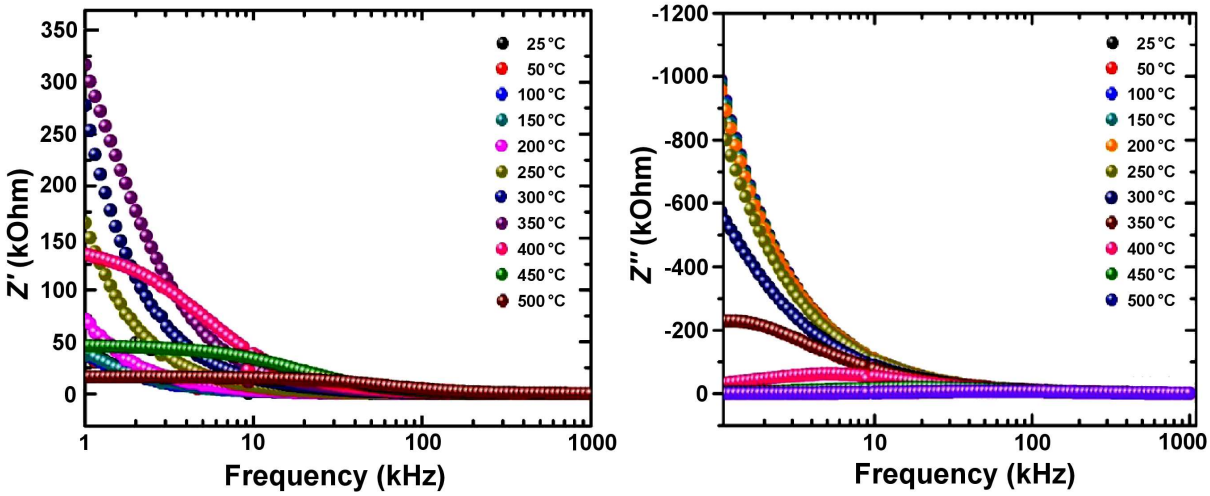

Figure 6. Variation of the real (a) and imaginary (b) part of impedance with frequency at selected temperatures from 25 to 500 °C

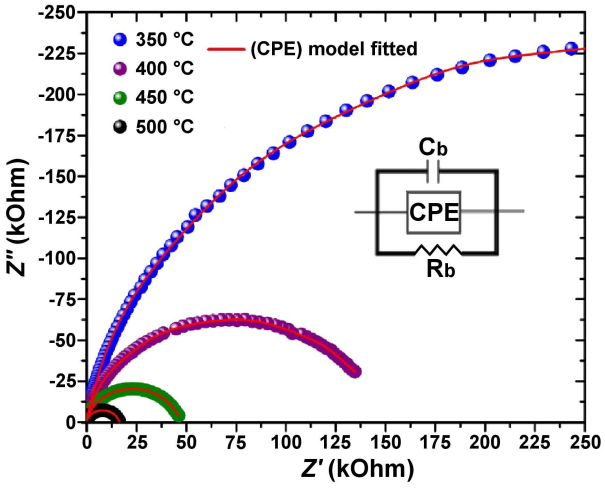

Figure 7. Fitted Nyquist plots

Table 1. The circuit parameters C_b, *CPE*, *CPE* power exponent (n) and R_b, obtained from equivalent circuit [47]

T [°C]	C_b [F/cm^2]	*CPE* [Fs^{n-1}/cm^2]	n	R_b [Ω/cm^2]
25	1.23×10^{-10}	2.72×10^{-9}	0.8	1.00×10^{15}
50	1.26×10^{-9}	1.58×10^{-10}	0.8	1.00×10^{15}
100	1.26×10^{-10}	1.58×10^{-10}	0.8	9.02×10^{14}
150	1.27×10^{-9}	1.74×10^{-10}	0.8	1.00×10^{15}
200	1.27×10^{-9}	1.74×10^{-10}	0.8	1.00×10^{15}
250	1.29×10^{-10}	2.42×10^{-9}	0.8	1.00×10^{15}
300	1.24×10^{-10}	3.21×10^{-9}	0.8	5.23×10^{6}
350	1.19×10^{-10}	2.59×10^{-9}	0.8	619100
400	1.12×10^{-10}	1.88×10^{-9}	0.8	152000
450	1.10×10^{-10}	1.45×10^{-9}	0.8	47170
500	1.14×10^{-10}	1.34×10^{-9}	0.8	16250

sons at higher temperatures. So, it may be concluded that the observed electrical conduction in the sample is related to the hopping of the electrons, oxygen ion vacancies and defects [43].

Figure 7 represents the Nyquist plots of the $PbFe_{1/3}Ti_{1/3}W_{1/3}O_3$ single perovskite compound in the temperature range from 350 to 500 °C. The presence of semi-circular curves in the Nyquist plots is due to the contribution of grains, which may influence the resistive and capacitive data of the given materials. An electrical circuit was designed taking resistive and capacitive passive elements (R, C, *CPE*) to calibrate the theoretical values of the measured electrical parameters. The above designed equivalent circuit has been modelled using ZSIMP WIN version 2 software packages [44,45]. Semicircular arc shows that the Debye-type relaxation is present in the sample. The fitted values of the bulk resistance (R_b) show that resistance of the sample decreases with the rise of temperature ensuring the NTCR behaviour [46] and semiconducting nature. The list of the electrical parameters, i.e. grain resistance (R_b), capacitance (C_b) and *CPE* power exponent (n) calculated using equivalent circuit ($C \parallel CPE \parallel R$) are represented in Table 1.

3.4. Conductivity

Figures 8a and 8b represent the variation of AC conductivity with frequency and temperature. The AC electrical conductivity of the prepared sample was calculated by the following equation:

$$\sigma_{AC} = \omega \cdot \varepsilon_r \cdot \varepsilon_0 \cdot \tan\delta \tag{1}$$

The hopping conduction mechanism is dominated over the band conductivity process in the material [48]. The activation energies of the sample at different frequency were calculated by the following equation:

$$\log\sigma = \log\sigma_0 - \frac{E_a}{2.303 k_B \cdot T} \tag{2}$$

where σ_0 is pre-exponential factor and k_B is the Boltzmann constant. A graph of $\log\sigma$ versus $(1/T)$ is plotted and slope of the plot is equal to $(-E_a/2.303k_B)$.

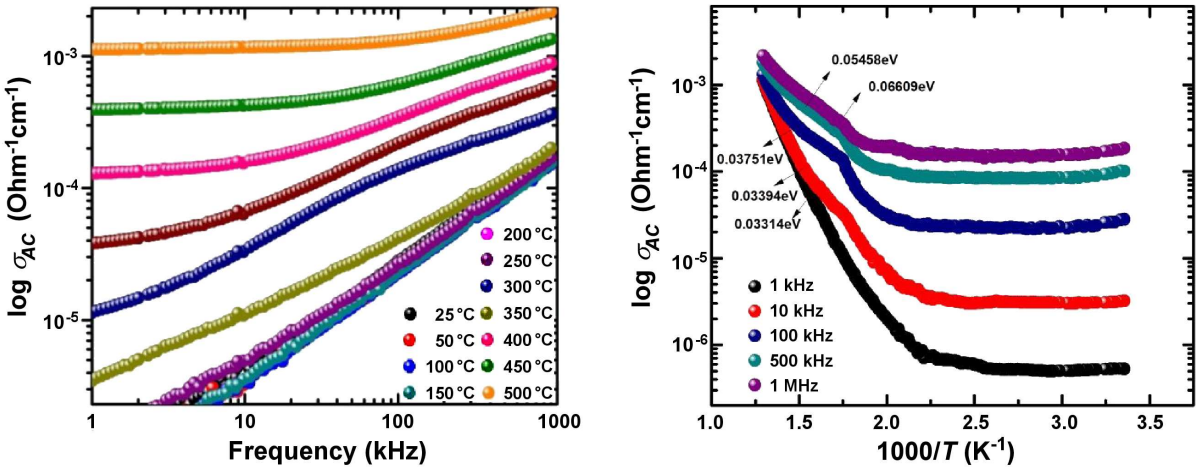

Figure 8. Variation of AC conductivity with frequency (a) and temperature (b)

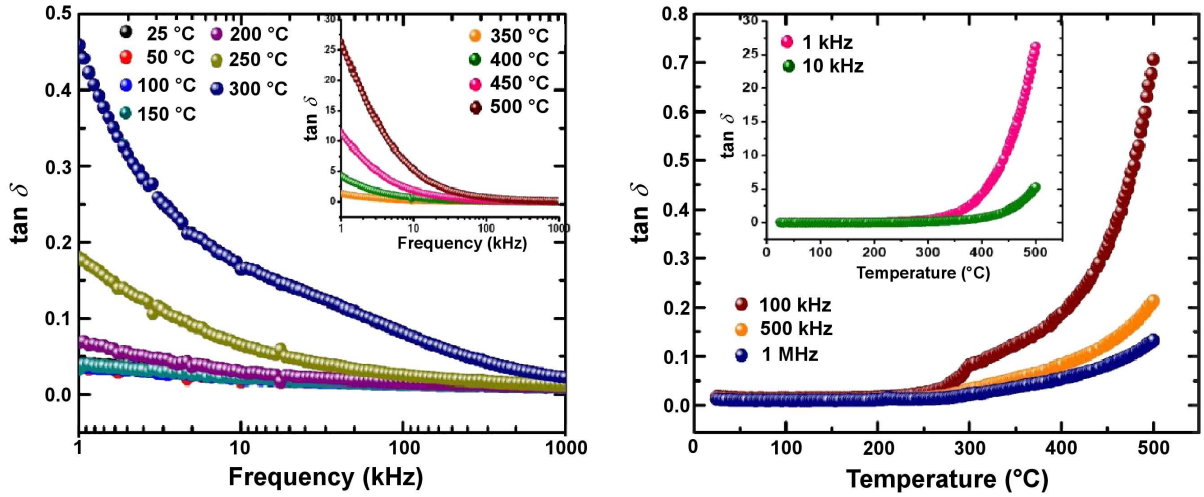

Figure 9. Variation of M' (a) and M'' (b) with frequency

The activation energies, in the temperature range from 240 to 480 °C, are 0.03314, 0.03394, 0.03751, 0.05458 and 0.06609 eV at 1 kHz, 10 kHz, 100 kHz, 500 kHz and 1 MHz, respectively.

Figures 9a and 9b show the variation of M' and M'' in a wide range of frequency. The material's conductivity, polarization and relaxation time can be evaluated from the data analysis of the electrical modulus, which is function of frequency and temperature. The real and imaginary parts of the modulus (M' and M'') can be calculated using the relations, where all terms have their usual meaning [49]:

$$M' = A\left[\frac{(\omega \cdot R \cdot C)^2}{1 + (\omega \cdot R \cdot C)^2}\right] \tag{3}$$

$$M'' = A\left[\frac{\omega \cdot R \cdot C}{1 + (\omega \cdot R \cdot C)^2}\right] \tag{4}$$

Due to the presence of crystal defects and inhomogeneous domains in the materials, electrical impedance plots are not useful to calculate the effect of grains and grain boundaries. Thus, electrical modulus plays an important role to calculate the effects of grain and grain boundaries in the materials. It is observed that the value of M' increases with the increase in frequency and merge into one line at high temperature, whereas the M'' decreases with the rise of frequency. Therefore, conclusion may be drawn that material undergoes a thermally activated relaxation process due to the presence of hopping charge carriers [50]. The symmetrical modulus plots agree with the results of the Debye-type behaviour in the material. Figure 10 represents the Cole-

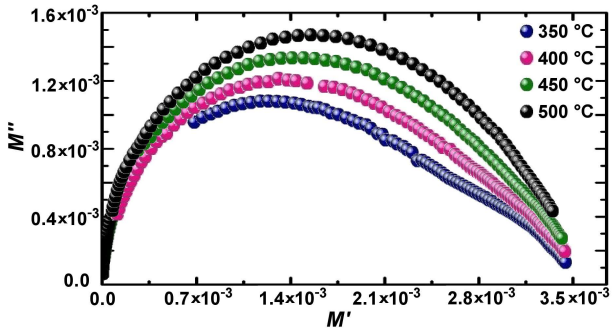

Figure 10. Cole-Cole plots

Cole plots for electric modulus of the PFTW single perovskite compound. The semicircular arcs of the Cole-Cole plots confirm that the prepared sample is semiconducting in nature [51,52].

IV. Conclusions

$PbFe_{1/3}Ti_{1/3}W_{1/3}O_3$ single perovskite compound was prepared and XRD profile shows that sample has orthorhombic structure with space group Pbam. Rietveld analysis gives refined lattice constants $a = 9.305$ Å, $b = 9.247$ Å, $c = 5.678$ Å and $\alpha = \beta = \gamma = 90°$. The FTIR analysis shows presence of Ti–O, W–O–W, Fe–O vibration stretching. This confirms that Fe^{2+} and W^{6+} ions are incorporated in the structure and most probably substituted Ti^{4+} ions at the B site of the perovskite ABO_3 structure. The semiconducting behaviour is observed following NTCR character confirmed from the dielectric spectra. The equivalent circuit ($C \parallel CPE \parallel R$) was used to model the impedance data and evaluate bulk resistance and capacitance. It was observed that grain resistance (R_b) of the sample decreases with the rise of temperature, which further supports the NTCR behaviour. The electrical modulus explains thermally activated relaxation process due to the presence of hopping charge carriers. The perfect semi-circular curves of the Cole-Cole plots confirm the semiconducting nature. Therefore, the prepared $PbFe_{1/3}Ti_{1/3}W_{1/3}O_3$ is semiconducting in nature and may be very useful in designing energy storage capacitors, sensors and actuators.

References

1. A. Bose, T. Maity, S. Bysakh, A. Seal, S. Sen, "Influence of plasma pressure on the growth characteristics and ferroelectric properties of sputter-deposited PZT thin films", *Appl. Surf. Sci.*, **256** (2010) 6205–6212.
2. D. Damjanovic, "Ferroelectric, dielectric and piezoelectric properties of ferroelectric thin films and ceramics", *Rep. Prog. Phys.*, **61** [9] (1998) 1267–1324.
3. I. Chilibon, C. Dias, P. Inacio, J. Marat-Mendes, "PZT and PVDF bimorph actuators", *J. Optoelectron. Adv. Mater.*, **9** [6] (2007) 1939–1943.
4. H. Fan, G.T. Park, J.J. Choi, H.E. Kim, "Preparation and characterization of sol-gel-derived lead magnesium niobium titanate thin films with pure perovskite phase lead oxide cover coat", *J. Am. Ceram. Soc.*, **85** [8] (2002) 2001–2004.
5. J.F. Scott, *Ferroelectric Memories*, Springer Series in Advanced Microelectronics. Springer, Berlin, 2000.
6. G. Sumara, "The relaxational properties of compositionally disordered ABO_3 perovskite", *J. Phys. Conds. Matter*, **15** (2003) R367–R370.
7. L.E. Cross, "Relaxor ferroelectrics: An overview", *Ferroelectrics*, **151** (1994) 305–309.
8. P.A. Cox, *Transition Metal Oxides: An Introduction to Their Electronic Structure and Properties*, Clarendon Press, 2010.
9. W. Kleemann, J. Dec, P. Lehnen, R. Blinc, B. Zalar, R. Pankrath, "Uniaxial relaxor ferroelectrics: The ferroic random-field Ising model materialized at last", *Europhys. Lett.*, **57** (2002) 14–18.
10. T. Granzow, "Change from 3D-Ising to random field-Ising-model criticality in a uniaxial relaxor ferroelectric", *Phys. Rev. Lett.*, **92** (2004) 065701.
11. R. Pirc, "Spherical random-bond–random-field model of relaxor ferroelectrics", *Phys. Rev. B*, **60** (1999) 13470–13473.
12. V. Bobnar, Z. Kutnjak, R. Pirc, R. Blinc, A. Levstik, "Crossover from glassy to inhomogeneous-ferroelectric nonlinear dielectric response in relaxor ferroelectrics", *Phys. Rev. Lett.*, **84** (2000) 5892–5892.
13. L.E. Cross, "Relaxor ferroelectrics", *Ferroelectrics*, **76** (1987) 241–267.
14. B.G. Lone, P.B. Under, S.S. Patil, P.W. Khirade, S.C. Mehrotra, "Dielectric study of methanol- ethanol mixtures using the TDR method", *J. Mol. Liq.*, **141** (2008) 47–53.
15. D. Viehland, S.J. Jang, L.E. Cross, M. Wuttig, "Deviation from Curie-Weiss behavior in relaxor ferroelectrics", *Phys. Rev. B*, **46** (1992) 8003–8007.
16. V.E. Colla, E.Y. Koroleva, N.M. Okuneva, S.B. Vakhrushev, "Long-time relaxation of the dielectric response in lead magnoniobate", *Phys. Rev. Lett.*, **74** (1995) 1681–1985.
17. Q. Jiang, X.F. Cui, M. Zhao, "Size effects on Curie temperature of ferroelectric particles", *Appl. Phys. A Mater. Sci. Proc.*, **78** (2004) 703–704.
18. M. Chandrasekhar, P. Kumar, "Processing and characterizations of BNT-KNN ceramics for actuator applications", *Process. Appl. Ceram.*, **10** [2] (2016) 73–77.
19. A. Levstik, Z. Kutnjak, C. Filipič, R. Pirc, "Glassy freezing in relaxor ferroelectric lead magnesium niobate", *Phys. Rev. B*, **57** (1998) 11204–11207.
20. G. Schmidt, H. Arndt, G. Borchhardt, J. von Cieminski, T. Petzsche, K. Borman, A. Sternberg, A. Zirnite, V.A. Isupov, "Induced phase transitions in ferroelectrics with diffuse phase transition", *Phys. Status Solid*, **63** (1981) 501–509.
21. R. Pirc, R. Blinc, "Spherical random-bond-random-field model of relaxor ferroelectrics", *Phys. Rev. B*, **60** (1999) 13470–13475.
22. V. Westphal, W. Kleemann, M.D. Glinchuk, "Diffuse phase transition and random-field induced domain states of the relaxor ferroelectric $PbMg_{1/3}Nb_{2/3}O_3$", *Phys. Rev. Lett.*, **68** (1992) 847–850.
23. H. Yao, K. Ema, C.W. Garland, "Non-adiabatic scanning calorimeter", *Rev. Sci. Instrum.*, **69** (1998) 172–179.
24. D. Grieger, M. Fabrizio, "Low-temperature magnetic ordering and structural distortions in vanadium sesquioxide V_2O_3", *Phys. Rev. B*, **92** (2015) 075121–075126.
25. A. Meklid, A. Boutarfaia, "The effects of sintering temperature and titanium ratio on structural and electrical properties of new PZT-CNS ceramics", *Model. Measur. Control C*, **79** (2018) 1–5.
26. O.A. Bunina, I.N. Zakharchenko, Yu.I. Golovko, V.M. Mukhortov, D.V. Stryukov, Yu.I. Yuzyuk, "Structural properties of composite thin films $BiFeO_3$-$Ba_{0.8}Sr_{0.2}TiO_3$", *Ferroelectrics*, **439** (2017) 67–73.
27. R.K. Parida, D.K. Pattanayak, B.N. Parida, "Impedance and modulus analysis of double perovskite Pb_2BiVO_6", *J. Mater. Sci. Mater. Electron.*, **28** (2017) 16689–16695.
28. S.K. Parida, J. Mohapatra, D.K. Mishra, "The structural and magnetic behavior of spinel $CuMn_2O_4$ synthesized by co-melting technique", *Mater. Lett.*, **181** (2016) 116–118.

29. B.N. Parida, R.K. Parida, A. Panda, "Multi-ferroic and optical spectroscopy properties of $(Bi_{0.5}Sr_{0.5})(Fe_{0.5}Ti_{0.5})O_3$ solid solution", *J. Alloys Compd.*, **696** (2017) 338–344.
30. Q. Hang, Z. Xing, X. Zhu, M. Yu, Y. Song, J. Zhu, Z. Liu, "Dielectric properties and related ferroelectric domain configurations in multiferroic $BiFeO_3$-$BaTiO_3$ solid solutions", *Ceram. Int.*, **38** (2012) S411–S414.
31. G. Fuxi, *Optical and Spectroscopic Properties of Glass*, Springer-Verlag, Berlin, 1991, p. 136.
32. M. Ganguli, K.J. Rao, "Structural role of PbO in Li_2O–PbO–B_2O_3 glasses", *J. Solid State Chem.*, **145** (1999) 65–76.
33. E.I. Kamitsos, M.A. Karakassides, G.D. Chryssikos, "Vibrational spectra of magnesium-sodium-borate glasses. 2. Raman and mid-infrared investigation of the network structure", *J. Phys. Chem.*, **91** (1987) 1073–1079.
34. G.J Blasse,"Vibrational spectra of solid solution series with ordered perovskite structure", *Inorg. Nucl. Chem.*, **37** (1975) 1347–1351.
35. C.J. Wright, "Inelastic neutron scattering spectra of the hydrogen tungsten bronze $H_{0.4}WO_3$", *J. Solid State Chem.*, **20** (1977) 89–92.
36. F. Daniel, B. Desbat, J.C. Lassegues, B. Gerand, M. Figlarz, "Infrared and Raman study of WO_3 tungsten trioxides and WO_3, xH_2O tungsten trioxide tydrates", *J. Solid State Chem.*, **67** (1987) 235–247.
37. J. Pfeifer, C. Guifang, P. Tekula-Buxbaum, B.A. Kiss, M. Farkas-Jahnke, K. Vadasdi, "A reinvestigation of the preparation of tungsten oxide hydrate WO_3, $1/3H_2O$", *J. Solid State Chem.*, **119** (1995) 90–97.
38. A. Delsemme, B. Rosen, "Spectre de FeO", *Bull. Soc. Roy. Sci. Liege*, **14** (1945) 70–80.
39. B. Rosen, "Spectra of diatomic oxides by the method of exploded wire", *Nature*, **156** (1945) 570–571.
40. A.J. Dos santos-García, E. Solana-Madruga, C. Ritter, A. Andrada-Chacón, J. Sánchez-Benítez, F.J. Mompean, M. Garcia-Hernandez, R. Sáez-Puche, R. Schmidt, "Large magnetoelectric coupling near room temperature in synthetic melanostibite Mn_2FeSbO_6", *Angew. Chemie Int. Ed.*, **56** (2017) 4438–4442.
41. L. Alexander, H.P. Klug, "Determination of crystallite size with the X-ray spectrometer", *J. Appl. Phys.*, **21** (1950) 137–142.
42. S. Hajra, M. Sahu, V. Purohit, R.N.P. Choudhary, "Dielectric, conductivity and ferroelectric properties of lead-free electronic ceramic: $0.6Bi(Fe_{0.98}Ga_{0.02})O_3$-$0.4BaTiO_3$", *Heliyon*, **5** [5] (2019) 01654–01667.
43. S.K. Dehury, P.G.R. Achary, R.N.P. Choudhary, "Electrical and dielectric properties of bismuth holmium cobalt titanate ($BiHoCoTiO_6$): A complex double perovskite", *J. Mater. Sci. Mater. Electron.*, **29** (2018) 3682–3689.
44. A.K. Jonscher, "The universal dielectric response", *Nature*, **267** (1977) 673–679.
45. A.K. Jonscher, "Dielectric relaxation in solids", *J. Phys. D. Appl. Phys.*, **32** (1999) R57–R59.
46. R. Ranjan, R. Kumar, N. Kumar, B. Behera, R.N.P Choudhary, "Impedance and electric modulus analysis of Sm-modified $Pb(Zr_{0.55}Ti_{0.45})_{1-x/4}O_3$ ceramics", *J. Alloys Compd.*, **509** [22] (2011) 6388–6394.
47. B. Hirschorn, M.E. Orazem, B. Tribollet, V. Vivier, I. Frateur, M. Musiani, "Constant-phase-element behavior caused by resistivity distributions in films", *J. Electrochem. Soc.*, **157** (2010) C452–C457.
48. S. Sen, R.N.P. Choudhary, P. Pramanik, "Structural and electrical properties of Ca^{2+}-modified PZT electroceramics", *Phys. B Condens. Matter*, **387** (2007) 56–62.
49. N.K. Mohanty, S.K. Satpathy, B. Behera, P. Nayak, R.N.P. Choudhary, "Complex impedance properties of $LiSr_2Nb_5O_{15}$ ceramic", *J. Adv. Ceram.*, **1** (2012) 221–226.
50. J.R. Macdonald, "Note on the parameterization of the constant-phase admittance element", *Solid State Ionics*, **13** (1984) 147–149.
51. S.K. Parida, R.N.P. Choudhary, P.G.R. Achary, "Structure and ferroelectric properties of lead nickel tungsten titanate: $Pb(Ni_{1/3}Ti_{1/3}W_{1/3})O_3$ single perovskite", *Ferroelectrics*, **551** (2019) 109–121.
52. S.K. Sinha, S.N. Choudhary, R.N.P. Choudhary, "Studies of structural, dielectric and electrical behavior of $Pb(Mn_{1/4}Co_{1/4}W_{1/2})O_3$ ceramics", *J. Mater. Sci.*, **39** (2004) 315–318.